Electronic Supplementary Information

Asymmetries in the Spread of Drops Impacting on Hydrophobic Micropillar Arrays

Simon Robson[a] and Geoff R. Willmott,*[ab]

[a] The Departments of Physics and Chemistry, The University of Auckland, New Zealand

[b] The MacDiarmid Institute for Advanced Materials and Nanotechnology

*Corresponding author

Email: g.willmott@auckland.ac.nz

1 Further Surface Characterization

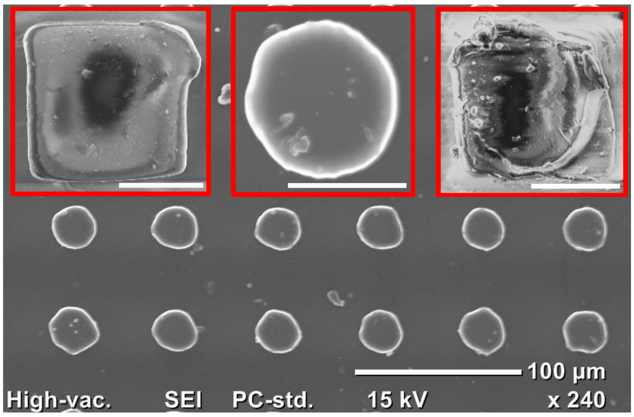

(a)

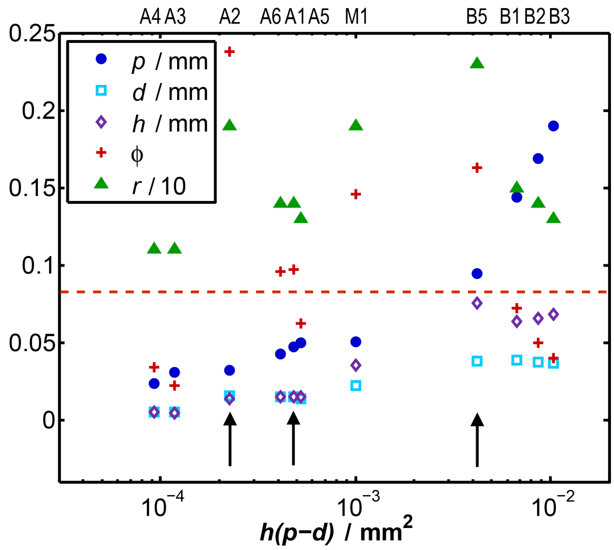

(b)

FIG. 1. Figure 1(a) is an SEM image of sample M1. Inset: typical single pillars with 20 μm scale bars from samples B5 (left, square), M1 (centre, circle), and B1 (right, rough square). Fig. 1(b) compares surface geometric characteristics from Table I, main text. The uncertainty in the corridor area $h\,(p-d)$ is smaller than the markers ($< 1\%$). Arrows indicate surfaces for which jetting was predominantly on-axis for all drop heights. Full microstructure penetration did not occur on those surfaces with values of ϕ above horizontal dashed line.

2 Drop Impact Outcomes

Based on our observations and previous literature, five classifications of the final outcomes were identified for the side view experiments. An example of each is shown in Fig. 2(a), with the ‘prompt splash’ described by Yarin[1] being prevalent at high We. ‘Attached sticky retraction’ is similar to Yarin’s ‘deposition’, but the rim is distorted by fingering and although the microstructure is fully penetrated, the drop does retract from its greatest extent. ‘Facile retraction’ is similar, but the rim retracts more quickly because only part of the microstructure has been penetrated. Facile retraction typically leads to some rebounding. The ‘partial rebound’ outcome is as defined by Yarin,[1] with a smooth rim shape observed. The microstructure is not fully penetrated, and the volume of rebounding liquid is greater than for facile retraction. Finally, the ‘sticky vibrating ball’ was defined by Tsai et al.,[2] and is observed for fully penetrated microstructures. The rim shape is not strongly distorted by fingers.

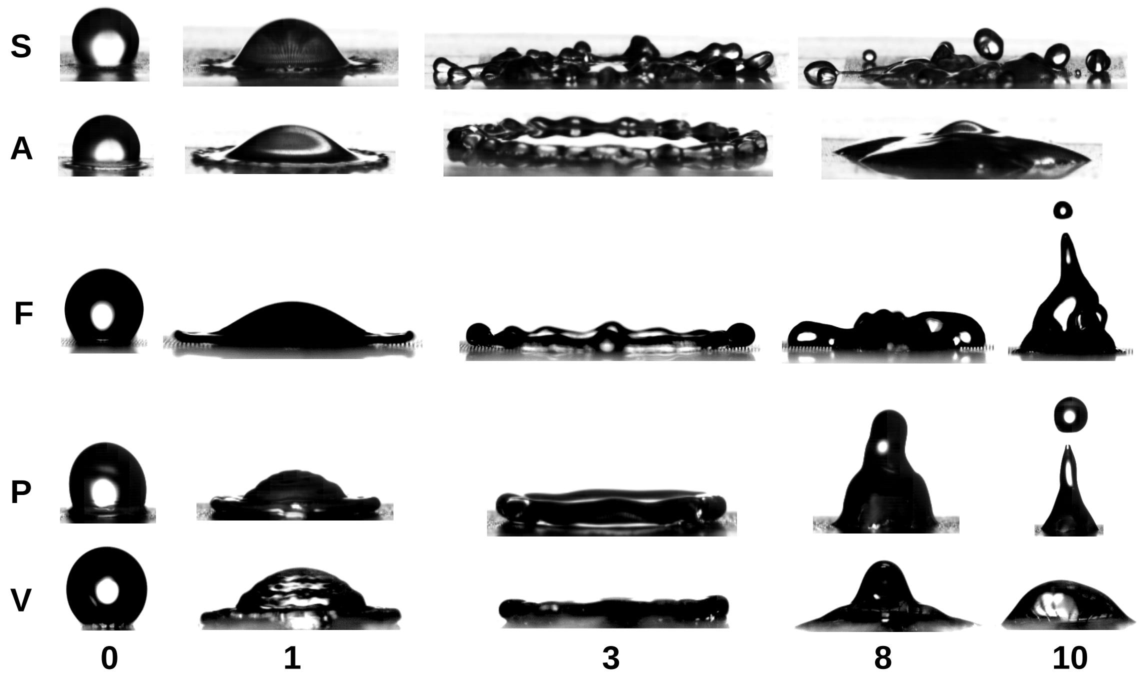

(a)

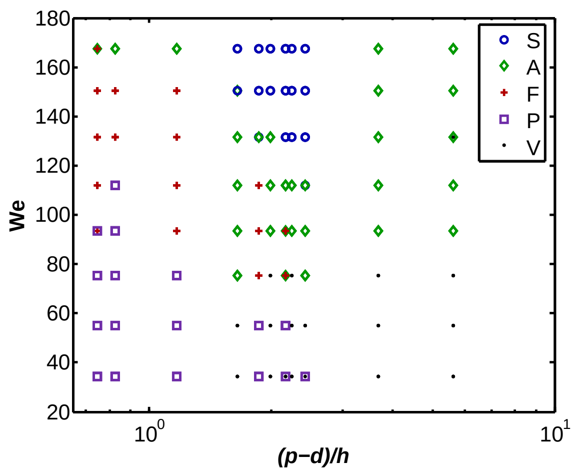

(b)

FIG. 2. Figure 2(a) demonstrates drop outcomes in rows of sequential images: prompt (S)plash (surface A1, We = 157); (A)ttached sticky retraction (A3, We = 132); (F)acile retraction (B5, We = 132); (P)artial rebound (A6, We = 34); (V)ibrating ball (B3, We = 34). Numbers at the base of each column indicate the approximate time in ms after impact. Figure 2(b) classifies outcomes as a function of We and surface geometry.

3 Spread of the Lamella with Time

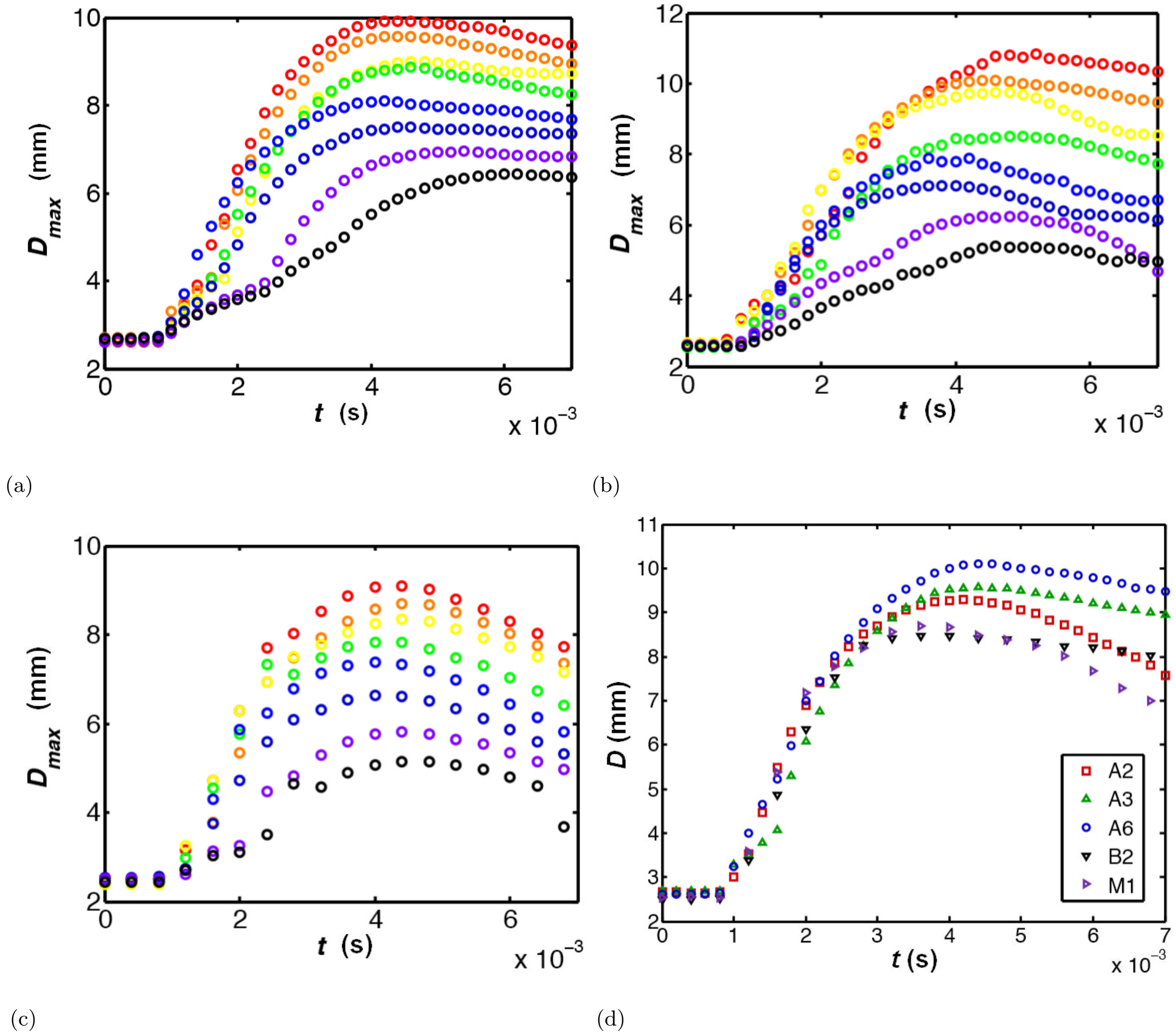

FIG. 3. Examples of the time evolution of the drop diameter D for impacts on surfaces A3 (Fig. 3(a)), A6 (Fig. 3(b)), and B5 (Fig. 3(c)). From bottom to top, We = 34, 55, 75, 93, 112, 132, 151, and 167. Figure 3(d) compares several surfaces at We = 151.

4 Jetting

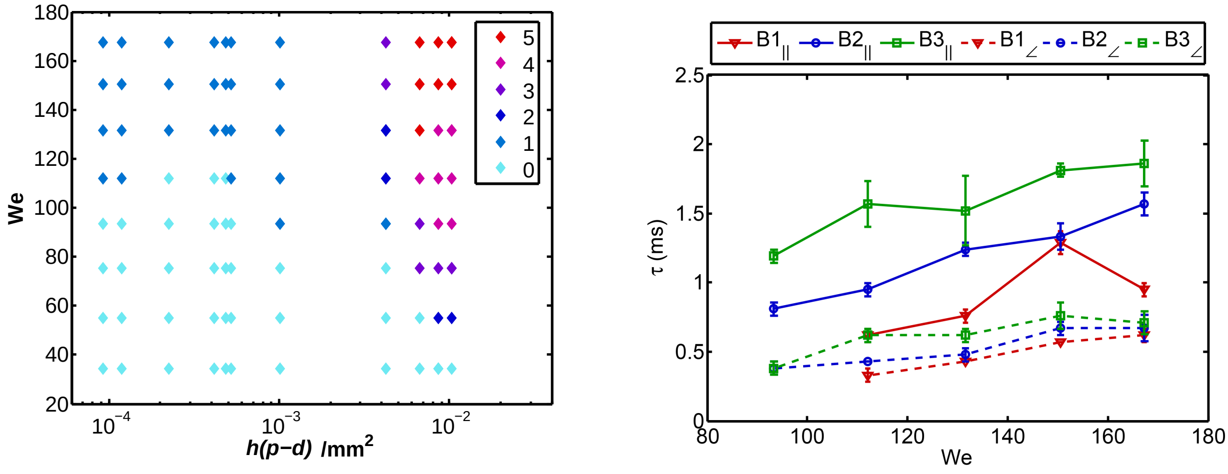

(a) (b)

FIG. 4. Figure 4(a) is a phase diagram indicating the overall intensity of jetting, classified empirically. Figure 4(b) plots the time (τ) between jet formation (identified in the frames immediately following impact) and the time at which jets detached to form a satellite drop, or else neighbouring jets coalesced to form a finger. Measurements are shown for three surfaces, for jets both parallel ($\|$) and at 45° ($\angle$) to the pillar pattern axis.

In Fig. 4(b), a higher value of τ indicates faster jetting, because coalescence to form a finger only occurs once the jets are overtaken by the advancing rim of the drop splash. τ is greater on-axis than diagonally for the surfaces shown. Correlation between the directions of a microstructural lattice and the drop outcome has been observed previously.[3,4]

Reyssat et al.[5] considered the inertial force on the liquid sheet due to the air velocity, obtaining a scaling of the jet velocity u by

$$u = \frac{\rho_{air}}{\rho_{water}} \frac{{D_0}^2 U}{h\,(p-d)}. \tag{1}$$

This equation predicts $u \propto \mathrm{We}^{0.5}$, or $\tau \propto \mathrm{We}^{0.5}$ if the rim velocity is approximately constant as suggested by SI Fig. 3. Experimental results suggest that τ is greater when the corridor area $h\,(p-d)$ is larger, which is opposite to the trend predicted in SI Eq. 1.

5 Maximum Spread

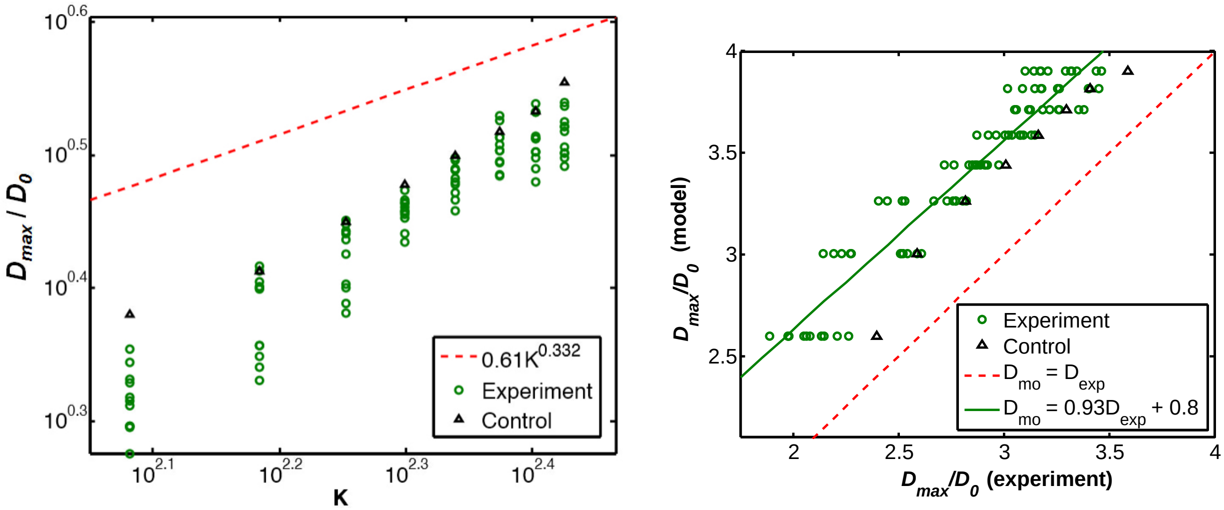

(a) (b)

FIG. 5. Comparison of experimental data with models for maximum spread. The red dashed lines correspond to agreement with the models proposed by Scheller and Bousfield[6] and by Roisman[7] in Figs. 5(a) and 5(b) respectively. The green line in Fig. 5(b) is a linear fit to the experimental data.

Scheller and Bousfield[6] proposed an empirical scaling argument of the form $D_{\max} = 0.61\mathrm{K}^{0.332}$ over the range $10 < \mathrm{K} < 1000$, where $\mathrm{K} = \mathrm{Re}^{1/2}\mathrm{We}^{1/4}$. This model systematically overestimated our results over the lower range of $120 < \mathrm{K} < 270$. A fit to the data to obtain the two empirical constants (Fig. 5(a)) suggests the relation $D_{\max} = 0.12\mathrm{K}^{0.605}$, and the two relations intersect at $\mathrm{K} \approx 385$. The difference between these relations is probably explained by the use of smooth polymer and glass surfaces in the experiments reported by Scheller and Bousfield,[6] who found no strong dependence on surface wettability.

Roisman[7] developed a semi-empirical model for the maximum spread based on the energy balance of a drop, with mass and momentum being conserved, and viscous effects being taken into account. The model given by the expression

$$D_{\max} \approx 0.87 Re^{1/5} - 0.40 Re^{2/5} We^{-1/2}$$

is compared with our results in Fig. 5(b). The maximum diameter is overestimated for all samples, including the control surface. Again, this study noted that the influence of wettability was minor but did not account for a microstructured surface.

6 Further Asymmetry Data

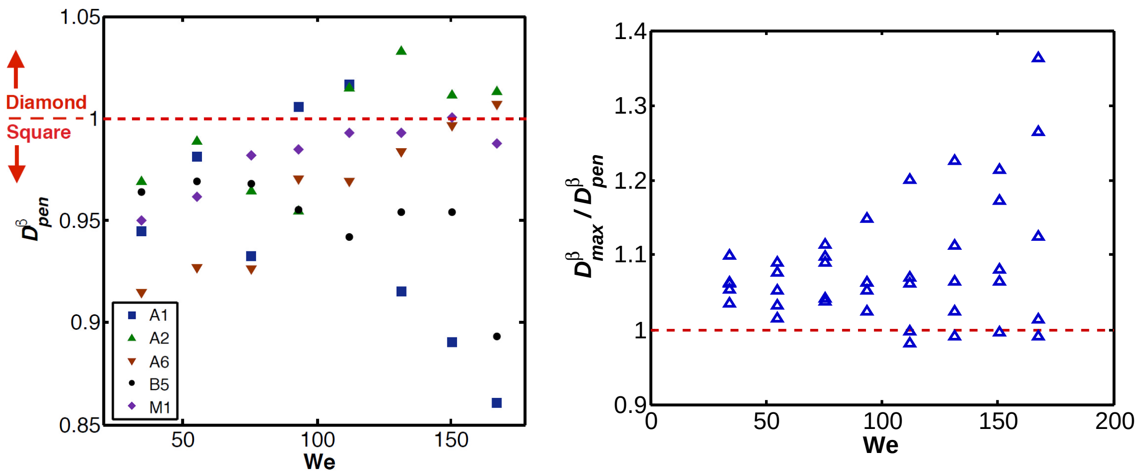

FIG. 6. Further asymmetry data on those five surfaces for which partial penetration of the microstructure was observed. Figure 6(a) plots the asymmetry of microstructural penetration profiles as a function of We. Figure 6(b) plots the ratio between the maximum spread and penetration asymmetries. The data predominantly lie above 1, demonstrating that maximum spread profiles tend to be more diamond-like, and penetration profiles tend to be more square-like. Vertical error bars (omitted for clarity) are typically ~3.2% and do not exceed 9.0%.

7 Fingers on Rectangular Arrays

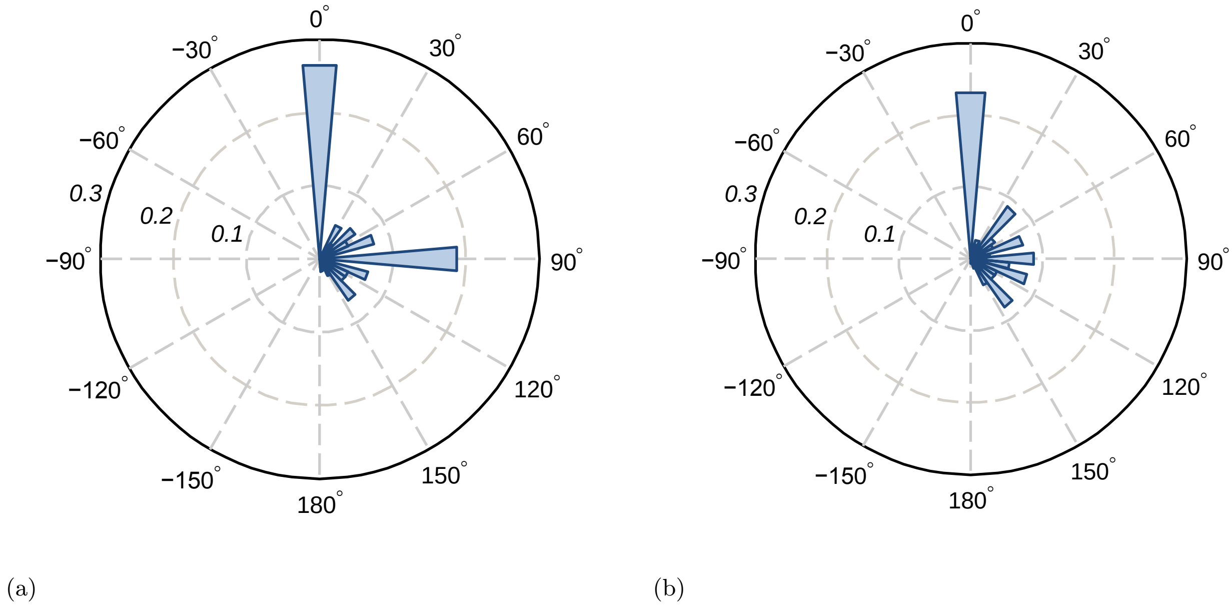

FIG. 7. Angular distribution of fingers on surfaces B2 (Fig. 7(a)) and B3 (Fig. 7(b)). The angles take a value between -5° and 175° relative to the pattern axes, and the length of each wedge indicates the population fraction (italic labels). The corridor area was greatest in the direction of the axis at 0°.

References

[1] A. L. Yarin, Annu. Rev. Fluid Mech. **38**, 159 (2006).

[2] P. Tsai, S. Pacheco, C. Pirat, L. Lefferts, and D. Lohse, Langmuir **25**, 12293 (2009).

[3] L. Xu, Phys. Rev. E **75**, 056316 (2007).

[4] P. Tsai, M. H. W. Hendrix, R. R. M. Dijkstra, L. Shui, and D. Lohse, Soft Matter **7**, 11325 (2011).

[5] M. Reyssat, D. Richard, C. Clanet, and D. Quéré, Faraday Discuss. **146**, 1 (2010).

[6] B. L. Scheller and D. W. Bousfield, AIChE J. **41**, 1357 (1995).

[7] I. V. Roisman, Phys. Fluids **21**, 052104 (2009).